PROPOSAL FOR A MODIFIED THOR LOWER ABDOMEN INCLUDING ABDOMINAL PRESSURE TWIN SENSORS

Sabine Compigne
Toyota Motor Europe NV/SA
Belgium

Mitsutoshi Masuda
Toyota Motor Corporation
Japan

Gaëtan Hanen
Philippe Vezin
François Bermond
Université de Lyon, Université Claude Bernard Lyon 1, IFSTTAR, LBMC UMR_T 9406
France

Paper Number 15-0216

ABSTRACT

This paper presents the evaluation of a modified THOR-NT lower abdomen which includes two abdominal pressure twin sensors (APTS®) as replacement for the displacement measurements. Further small changes such as the addition of small masses in front of the abdomen have also been made to better mimic the response of the PMHSs under seat belt loading. As a result, the biofidelity of the prototype abdomen was improved compared to THOR-NT standard abdomen. The addition of the small masses succeeded in increasing the initial peak force of the force-penetration response under seat belt tests. In rigid bar impacts, the prototype force-deflection response stayed longer in the corridor. The pressure measurement was repeatable and discriminated the various impact speeds as well as the impact direction. The pressure peaks were proportional to force and penetration peaks. This study demonstrates the feasibility of introducing the APTSs into THOR lower abdomen and makes proposals for further biofidelity enhancements.

INTRODUCTION

The Test Device for Human Occupant Restraint (THOR) is an advanced anthropomorphic test device designed to represent the automotive occupants in the sophisticated restraint systems, such as force-limited three-point belts and air bags. The first THOR version, THOR alpha, was released in 2000. Since then the dummy version has evolved into THOR-NT (NHTSA, 2005), THOR Mod Kit (Ridella et al., 2011) and THOR Metric (Parent, 2014). The current study focuses on the THOR lower abdomen which design has not changed along THOR versions except for the instrumentation. THOR abdomen biofidelity specifications are defined for a 6.1 m/s rigid-bar test simulating an impact to the lower rim of the steering wheel as previously tested by Cavanaugh et al. (1986) on Post Mortem Human Subjects (PMHSs). However, the seatbelt is reported nowadays as the most common abdominal injury source of belted occupants involved in a frontal collision (Huelke et al., 1993; Klinich et al., 2008). Rear seat occupants are especially concerned since they are reported to have a significantly higher rate of sustaining a moderate or severe abdominal injury compared to front seat occupants (Lamielle et al., 2006; Martin et al., 2010; Frampton et al., 2012). Several biomechanical studies investigated swine (Miller et al., 1989; Kent et al., 2008) or human abdomen responses (Hardy et al., 2001; Trosseille et al., 2002; Foster at al., 2006; Lamielle et al., 2008) under seatbelt loading which allow the evaluation of the dummy response. Some of the mentioned biomechanical studies investigated various abdominal injury predictors such as abdominal compression, belt tension, penetration speed, viscous criterion, force "viscous criterion", work of belt tension. Arterial and venous pressure peaks have also been proposed to serve as injury predictor of abdominal organs (Miller et al., 1989; Ruan et al., 2005; Kremer et al. 2011). Beillas et al. (2012) demonstrated the ability to measure pressure inside child Q-dummy abdomen using the Abdominal Pressure Twin Sensors (APTS®). The APTSs could detect injurious abdominal loading for child Q3 and Q6 dummies with an estimated risk of sustaining an AIS3+ abdominal injury of 50% at 1.09 bars. Hanen et al. (2011, 2012), Masuda et al. (2012) investigated the introduction of the APTSs inside the THOR lower abdomen. This paper presents the results of the prototype delivered in 2012 and developed from THOR-NT dummy version.

MATERIAL AND METHOD

THOR lower abdomen prototype

THOR-NT lower abdomen is made of two foam blocks and of an internal mounting weld assembly enclosed in a Cordura nylon bag. Two DGSPs (Double Gimbaled String Potentiometer) go through two holes in the foam blocks. They are attached to the rear on each side of the spine to mounting brackets and to the front of the abdominal bag. The DGSPs measure the three dimensional displacements of the two points on the bag surface. The whole lower abdomen assembly can be accessed by opening a zipper placed on the abdomen bag (NHTSA, 2005) (Figure 1).

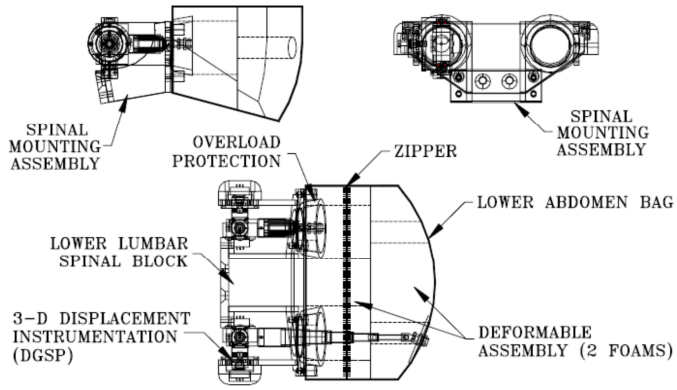

Figure 1. THOR-NT lower abdomen assembly (NHTSA, 2005).

The THOR lower abdomen prototype is made from THOR-NT abdomen components. An exploded view of the prototype assembly is shown in Figure 2. New front and rear foam blocks were ordered without holes as DGSPs are not used anymore. Instead two new vertical holes of 51 mm diameter with center axes spaced by 90 mm were made in the front foam block to receive the APTSs (Figure 3). The APTSs (version 2) were inserted with their caps downwards. The version 2 is composed of a 50 mm diameter soft polyurethane bladder filled with paraffin oil. The APTS has one cap through which oil is entered using a pressure column to provide consistent filling conditions. Pressure measures are made by XPR30 subminiature pressure sensors (Measurement Specialties, Les Clayes, France) placed in the balled cap at the interface with the oil (Beillas et al., 2012). Mounting brackets to the spine and abdomen internal plate geometries were simplified. The brackets allow a simpler mounting and dismounting of the entire abdomen assembly from the spine (Figure 4, Figure 5). The wires of the APTSs exit from the bottom of the front foam, go through two cuts made in the rear foam and finally pass through the holes of the modified internal plate and the abdomen bag.

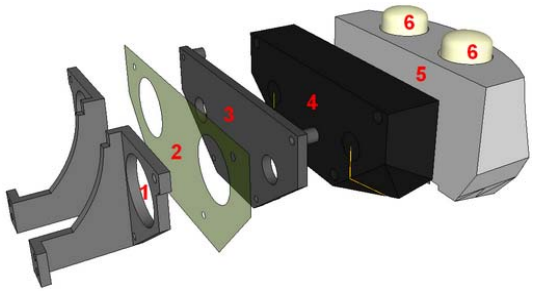

Figure 2. Abdomen prototype exploded view: (1) Right and left modified mounting brackets (2) Cordura bag (3) Modified internal plate (4) Rear foam block (5) Front foam block (6) Right and left APTSs.

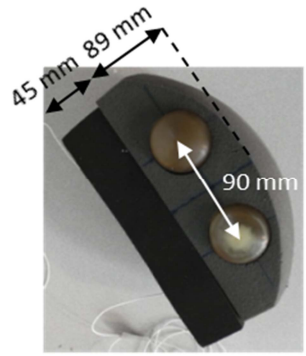

Figure 3. Top view of abdomen prototype equipped with the APTSs (dimensions measured from dummy parts) .

Figure 4. Standard (top) and modified (bottom) abdomen internal plate.

Figure 5. Standard (top) and modified (bottom) mounting bracket to the spine.

Fifteen steel cylinders of 30 mm diameter and 10 mm thickness are attached to the front of the abdomen bag using a Velcro® layer (Figure 6). They represent an additional mass of 825 g. The total mass of the prototype with the attachment brackets is 3.12 kg (THOR-NT abdomen assembly is 2.60 kg). The prototype abdominal depth is 292 mm and 282 mm without the small masses. This has to be compared with the THOR-NT abdominal depth of 265 mm. The abdomen prototype can similarly be mounted on THOR Mod Kit and THOR-Metric thanks to similar lower abdomen/spine assemblies between the dummies.

Figure 6. Abdomen prototype assembly with the small masses attached to the Cordura bag.

Test set-ups

The abdomen prototype response was evaluated under rigid bar impact and seatbelt loading as performed previously by Hanen at al. (2011) on THOR-NT standard abdomen. Its response was compared to available Post Mortem Human Subject (PMHS) corridors and standard THOR-NT abdomen response re-analysed from Hanen et al. (2011). Additional tests at various speeds (1 to 6.1 m/s) and different impact angles (0° and 20°) were performed to evaluate the sensitivity of the APTS measurement.

Rigid bar impact The THOR-NT dummy equipped with the abdomen prototype was submitted to 32 kg impactor tests according to Cavanaugh et al. (1986) test set-up. The impactor was equipped with a 25 mm diameter rigid bar of length 300 mm. Initial impact speed was varied from 1 to 6.1 m/s. The dummy was placed on a table covered by a Teflon® sheet with outstretched legs. The lumbar spine joint was in slouch position (9° between lumbar bracket and pelvis bracket) and the back was unsupported. The hands were attached at the head level. The table height was adjusted to align the rigid bar with the line joining the centers of the attachment nuts of the DGSPs (Figure 7).

The impactor was instrumented with a 20 kN SEDEME SAM-load cell and a 100 g ENTRAN EGCS-S067 uniaxial accelerometer. A light gate measured the impact speed just prior to the contact between the impactor bar and the dummy. The THOR dummy pelvis was instrumented with a 250 g ENTRAN EGAS-S077B three-axis accelerometer. A laser ODS 1150 (900 mm range, 0.1 mm resolution) was positioned in the back of the dummy and measured its pelvis displacement. Data acquisition was made at 20 kHz using Kistler acquisition system and channels were filtered according to SAE J211 using a low pass band Butterworth filter (CFC180 for the accelerations, pressures and laser displacement, CFC600 for the force).
Two high-speed cameras (Photron SA3 black and white) recorded the impact at a rate of 2000 frames/s with a resolution of 1024×1024 pixels. One camera filmed the overall scene and the other one was placed perpendicular to the dummy sagittal plane to measure the impactor and dummy pelvis displacements using Motion Track® software. The time "zero" was identified on the video by a flash which was lit up when the rigid bar came in contact with the dummy suit.
Impact force could be obtained by multiplying the impactor longitudinal acceleration by its mass (32 kg) or by the impactor load cell once corrected for the mass placed in front of the sensor (2.62 kg). Consistency of the force response obtained by these two means was checked. Abdomen penetration was measured as the difference between the impactor displacement and the one of the dummy pelvis obtained by the video analysis. Consistency with other measurements (difference of the double integration of impactor and dummy pelvis longitudinal accelerations) was also checked.
Abdominal penetration measured from the video was re-sampled using linear interpolation at 20 kHz to draw the force-penetration response.

Seatbelt loading The THOR-NT dummy equipped with the abdomen prototype was submitted to seatbelt loading according to Foster at al. (2006) test set-up. The dummy was seated on the floor covered by a Teflon® sheet with the legs outstretched and the back against a vertical rigid plate. The dummy lumbar spine joint was in slouch position and its arms were attached to the vertical structure at the head level. The seatbelt was wrapped around the abdomen at mid height and guided from the lateral aspects of the dummy abdomen. The same pretensioner systems as in Foster et al. (2006) study were used and denoted similarly Type A, B and C. Type B and C consisted of a single pretensioner (at different levels of pretension, respectively) whereas Type A consisted of two Type B pretensioners. In addition to Foster's configurations, two Type C pretensioners were also tested. In the case of a single pretensioner system, the webbing was attached on itself using a clamp whereas in the case of a dual pretensioner system, a webbing piece was wrapped around the dummy and its extremities were sewn to each pretensioner webbing. The longitudinal position of the pretensioner support was adjusted to set an initial small tension inside the webbing (10 to 20 N) (Figure 8).
Two 500 g ENTRAN EGAS-S077D uniaxial accelerometers were mounted on each side of the webbing together with two 16 kN MEAS EL20-S458 seatbelt load cells. The same laser as in the rigid bar impact was positioned in front of the dummy and targeted the dummy umbilicus. The dummy pelvis was instrumented with a 250 g ENTRAN EGAS-S077B three-axis accelerometer. Data acquisition was made at 20 kHz using Kistler acquisition system and channels were filtered according to SAE J211 using a low pass band Butterworth filter (CFC180 for the accelerations, pressures and laser displacement, CFC600 for the force).
Two Photron high-speed cameras recorded the impact at a rate of 2000 frames/s. One camera was placed in front of the dummy and the other one was placed to the right of the dummy, perpendicular to the dummy sagittal plane to record the seatbelt and the dummy pelvis displacements. Motion Track® software was used to perform the video analysis. The time "zero" was identified on the video by a flash which was lit up when firing the pretensioner.
Applied force to the abdomen was obtained by adding the forces recorded by both seatbelt load cells. Abdomen penetration was measured as the difference between the seatbelt displacement at dummy umbilicus level and the displacement of the dummy pelvis obtained by the video analysis. Consistency with other measurements (abdominal displacement measured by the laser and pelvis displacement obtained by the double integration of the pelvis longitudinal acceleration) was also checked.
Abdominal penetration measured from the video was re-sampled using linear interpolation at 20 kHz to draw the force-penetration response.

The prototype abdomen responses were overlaid in each test configuration with THOR-NT standard abdomen and, when available, with PMHS corridors. Dummy responses under rigid-bar impacts were compared with Cavanaugh et al. (1986) and Hardy et al. (2001) PMHS corridors defined using average force-penetration responses firstly filtered at 100 Hz and CFC60 respectively and scaled to a 76 kg subject using Eppinger

(1976) equal-stress/equal-velocity technique. Dummy responses under seatbelt loadings were compared with Foster et al. (2006) PMHS corridors defined using average force-penetration responses firstly filtered at CFC600 and scaled to a 78 kg subject using Eppinger (1976) equal-stress/equal-velocity technique.
In all studies, the corridors were calculated from the average response plus and minus one standard deviation. The linear approximations of corridors established in Hardy's and Foster's papers are used here. Cavanaugh's corridor was digitised from the paper.

Figure 7. Rigid bar impact test set-up.

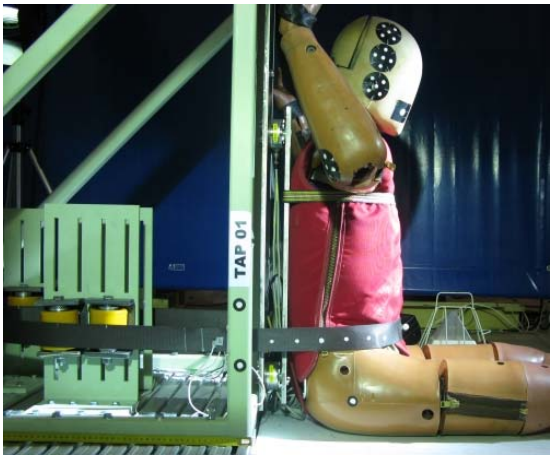

Figure 8. Seatbelt loading test set-up.

Test matrices Rigid bar impacts were performed with impact speeds ranging from 1 to 6.1 m/s. Each test condition was at least repeated twice. Oblique impacts at 20° towards the right side of the dummy were also conducted at 3 m/s impact speeds to assess directional sensitivity. One test at 3 m/s was performed without the prototype front masses to quantify their effect. The prototype abdomen response was compared to the standard abdomen one at 3 and 6.1 m/s impact speeds (Table 1).

Table 1. Rigid bar impact test matrix.

Test Id (Prototype abdomen)	Velocity (m/s)	Impact angle (°)	Test Id (Standard abdomen, Hanen et al., 2011)
TME82, 83	1	0	NA
TME84, 85	2	0	NA
TME79, 80, 81[(1)]	3	0	TME02, 03
TME77, 78, 88, 89	3	20	NA
TME90, 91	4	0	NA
TME92, 93	5	0	NA
TME94, 95	6.1	0	TME04, 05

[(1)]The masses in front of the abdomen were removed.

Seatbelt tests were conducted according to Table 2. Four loading conditions were applied to the abdomen. Each test condition was at least repeated twice. The prototype abdomen response was compared to the standard abdomen one under Type B and C test conditions.

Table 2. Seatbelt test matrix.

Test Id (Prototype abdomen)	Loading type	Test Id (Standard abdomen)
TAP39, TAP40	C	TAP04, TAP05
TAP41, TAP42, TAP47[(2)]	B	TAP02, TAP03
TAP43, TAP44	2×C	NA
TAP45, TAP46	A (2×B)	NA

[(2)]The masses in front of the abdomen were removed.

RESULTS

Prototype biofidelity

Rigid bar impact Figure 9 shows the force-time and the penetration-time responses of the standard and the prototype abdomen under 6.1 m/s rigid bar impact. The changes in force-time slopes and small peaks were correlated with the events observed on the video. Overall, the force peaks recorded for the standard abdomen are higher than those of the prototype abdomen and the penetration peaks are slightly higher for the prototype.
The first slope of the force curve of the standard abdomen is related to the abdomen jacket and front foam compression whereas in the prototype, the addition of the small masses gives first a steeper rise of the force during approximately the first 10 mm of penetration. At around 13 ms, the impactor hits the pelvis flesh of the dummy equipped with the standard abdomen. The effect of this contact is visible on the force slope of the standard abdomen due to the stiffness difference between the front abdomen foam and the pelvis flesh. At the moment the impactor slides over the flesh pelvis, the force drops suddenly for the standard abdomen and the penetration continues to increase. The impactor starts to move the dummy at around 27-30 ms, almost 10 ms after the force peak.
The contact with the pelvis flesh happened later with the prototype abdomen (at around 21 ms, 8 ms later than the standard abdomen). The compression of the APTS which happened in addition to the flesh compression increased more gradually the force before the impactor contacts the pelvis flesh. The force peak and the start of the dummy motion happened almost at the same time. The penetration peak occurred around 6 ms after the force peak due to the fact that the impactor continued to move inside the dummy after going above the pelvis flesh. By looking at the movie, this phenomenon was related to the impactor rigid bar mounting which was not sufficiently reinforced to avoid the impactor upwards bending due to the abdomen /pelvis reaction force (Figure 10). The movie showed that the impactor bar slid along the pelvis flesh whereas for the standard abdomen, a significant compression of the pelvis flesh was seen before the impactor could ride above it. For the prototype abdomen, it is expected that such ride off the pelvis flesh may not happen for a more rigidly mounted impacting face and therefore, the maximum penetration would correspond to the maximum force and would likely be lower.

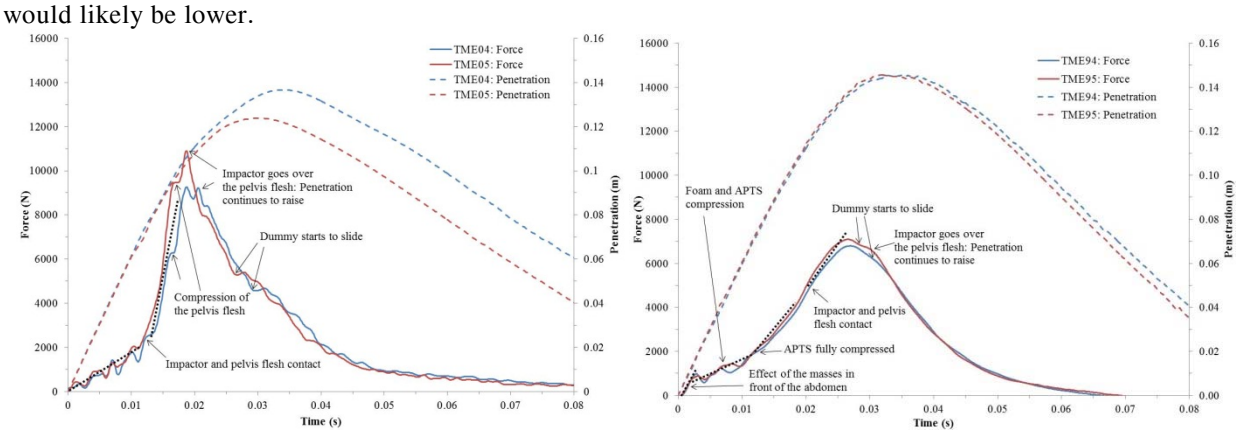

Figure 9. Force-time and Penetration-time responses of the standard (left) and the prototype (right) abdomen for 6.1 m/s rigid bar impact.

The difference in time for the impactor contact with the pelvis flesh between the standard and the prototype abdomens was mainly due to their abdomen width difference. Figure 11 shows both abdomens in front of the impactor. By looking at the jacket profile, it is visible that the prototype abdomen protrudes more outside of the pelvis flesh. The small masses and the APTS increase the prototype depth whereas in the standard abdomen, the DGSPs attached at the front of the abdomen bag compress the front foam. Approximately an additional 45 mm penetration was measured at the time of impactor-pelvis contact in the case of the prototype compared to the standard abdomen.

Figure 10. Impactor rigid-bar upwards bending.

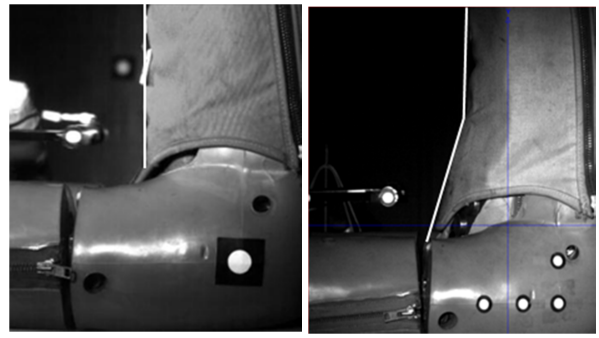

Figure 11. Depth of standard abdomen (left) and prototype abdomen (right).

Figure 12 and Figure 13 show the force-penetration responses of the two abdomens. Peak values are reported in Table 3. At 3 m/s, no contact was recorded between the impactor and the pelvis flesh for the dummy equipped with the prototype abdomen. On the opposite, this contact occurred at around 33 ms (88 mm penetration) with the standard abdomen. This increased the force peak (Figure 12). At 6.1 m/s, the prototype abdomen response stayed a bit longer in the PMHS corridors. This was due to a later contact with the pelvis flesh (at 119 mm penetration compared to 80 mm for the standard abdomen). Before that point, between 90 and 120 mm penetration (front foam block and APTS were fully compressed), the response of the prototype exceeds the upper bound of the PMHS corridor which seems to highlight a too stiff response of the abdomen rear foam block (Figure 13).

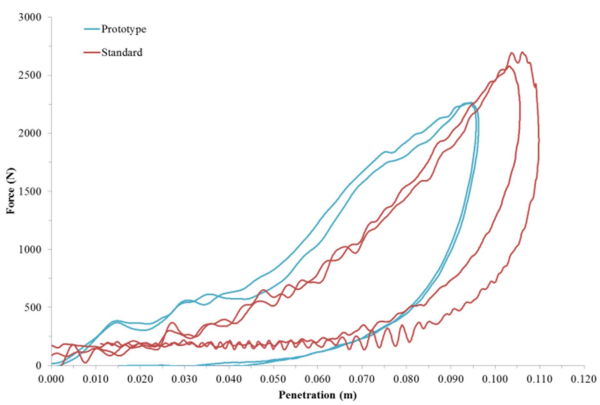

Figure 12. Force-penetration of the standard (in red) and prototype (in blue) abdomens at 3 m/s rigid bar impact.

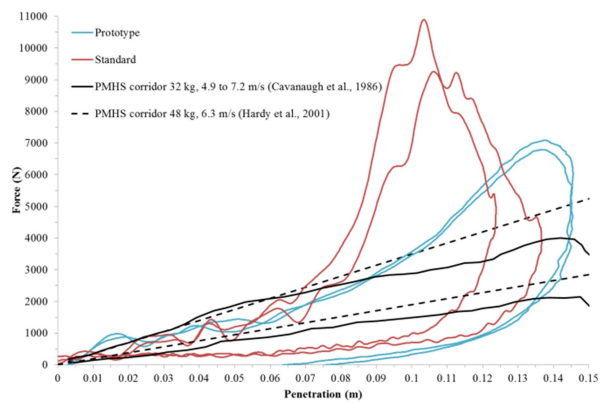

Figure 13. Force-penetration of the standard (in red) and prototype (in blue) abdomens overlaid with the scaled PMHS corridor at 6.1 m/s rigid bar impact.

Table 3. THOR-NT and Prototype peak values under rigid-bar impacts.

	Force Peak (N)		Penetration Peak (mm)	
Velocity (m/s)	**NT**	**Prototype**	**NT**	**Prototype**
3	2578 / 2699	2263 / 2265	106 / 110	96 / 96
6.1	9255 / 10902	6791 / 7088	137 / 124	146 / 146

Seatbelt loading Figure 14 and Figure 15 overlay the force-penetration responses of the standard THOR-NT abdomen, the prototype abdomen, the responses of a single PMHS (for Type C) and the PMHS corridors as defined by Foster et al. (2006) (for Type B and A). On Figure 14, the large force variations seen from 8 to 12 mm penetration were attributed to the left seatbelt sensor. The reason for these sudden variations is unknown and could not be checked from the video as the camera was on the right side of the dummy. Generally, the force measured at the webbing is increased for the prototype compared to the standard abdomen. However, this increase is still not sufficient to match PMHS responses. The penetration is also much lower than that of the PMHSs (Table 4). Foster et al. (2006) obtained 25%, 35% and 55% PMHS abdominal compression for

pretensioner Type C, B and A respectively, whereas 8%, 20% and 28% abdominal compression was reached with the abdomen prototype (292 mm abdominal depth is considered for the abdomen prototype). The standard abdomen gave similar compression to the prototype: 6% and 18-19% under pretensioner Type C and B (265 mm abdominal depth is considered for THOR-NT).

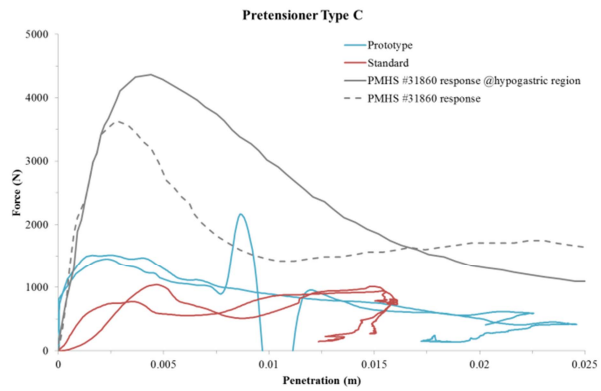

Figure 14. Force-penetration response of the standard and prototype abdomen compared to Foster et al. (2006) PMHS scaled responses (seatbelt load CFC180 versus penetration CFC60) for pretensioner Type C.

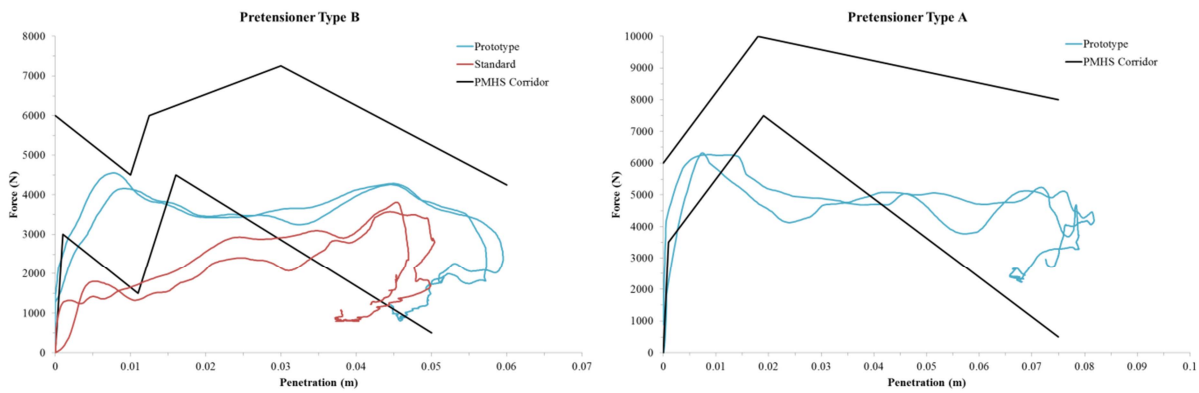

Figure 15. Force-penetration response of the standard and prototype abdomen compared to Foster et al. (2006) PMHS scaled corridors for pretensioners Type B (left) and A (right, only prototype).

Table 4. THOR-NT, Prototype and PMHS peak values under pretensioners Type C, B, A.

	Force Peak (N)			Penetration Peak (mm)		
Loading Type	**NT**	**Prototype**	**PMHS (Scaled)**	**NT**	**Prototype**	**PMHS (Scaled)**
C	939 / 1039	1451 / 1513	4363 / 3636	16.1 / 15.9	24.6 / 22.6	63.6 / 66.1
B	3573 / 3811	4257 / 4551	5593/5128/6726	50.4 / 47	57.3 / 59.5	97.6/93.6/107.4
A	NA	6318 / 6265	8289 / 7938 9737 / 9370	NA	78.9 / 81.8	123.6 / 112.1 153.2 / 128.5

<u>Effect of the APTS and small masses</u> Force-compression responses of the standard abdomen, of the prototype abdomen without the small masses, and of the prototype with the small masses are compared in Figure 16 and Figure 17 under rigid bar impact and pretensioner loading respectively. Compression is considered here to take into account the differences in abdomen depth between the THOR-NT (265 mm), the prototype without the small masses (282 mm) and the prototype abdomen (292 mm). Starting from the THOR-NT response, the addition of the APTS and of the small masses allowed the gradual increase of the force. The compression of the three abdomens is similar under the Type B seatbelt loading and smaller for the prototype under the 3 m/s rigid bar impact.

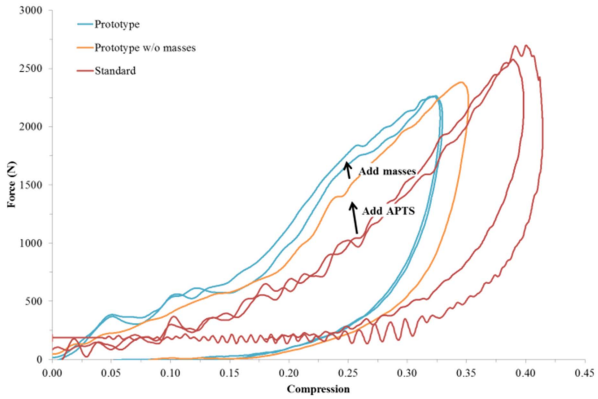

Figure 16. Force-compression responses of THOR-NT abdomen, prototype without small masses and prototype under 3 m/s rigid bar impact.

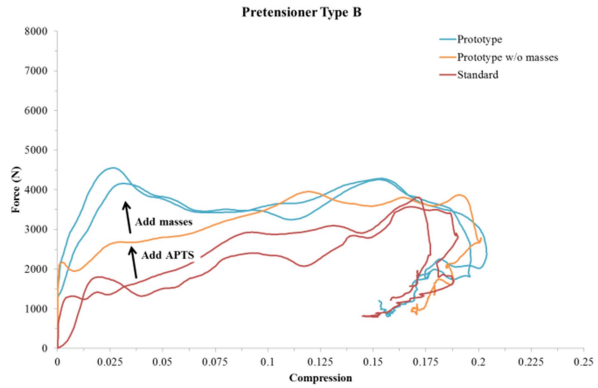

Figure 17. Force-compression responses of THOR-NT abdomen, prototype without small masses and prototype under pretensioner Type B loading.

Sensitivity to speed

Figure 18 shows the force-penetration responses of the prototype abdomen under 32 kg rigid-bar impacts and for speed variations between 1 and 6.1 m/s. The force and the penetration peaks raise with increasing speed. The force peaks vary between 400 and 7100 N and the penetration peaks vary between 46 mm and 145 mm. The loading slope also increases with the increased penetration at higher speed due to the compression of abdomen components. The contact between the rigid-bar and the pelvis flesh only occurred at 6.1 m/s. For 4 and 5 m/s impacts, the rigid bar rode over the pelvis flesh without touching it. This explains why the penetration peak occurred after the force peak. This kind of behaviour would not be expected with a reinforced rigid bar and in that case, the loading force would increase with a steeper slope up to the peak. Figure 19 overlays the force-penetration responses of the prototype for the various pretensioner types. The average retraction speeds of the seatbelt measured by video analysis using the targets placed on the side of the webbing are mentioned in the figure key. The retraction speed varied from 6.5 to 16 m/s. A first force peak is observed on all the curves at the very beginning of the penetration (at 2 and 10 mm for the slower and the higher retraction speed respectively). For Type B and A, this initial peak is followed by a decrease in force and a plateau almost up to the maximum penetration. For Type C and 2C, the force decreases after the initial peak until the maximum penetration. The force and the penetration peaks are increased with the retraction speed. A large jump in absorbed energy (area under force-penetration curves) is seen between Type 2C and B from 50 to 200 J.

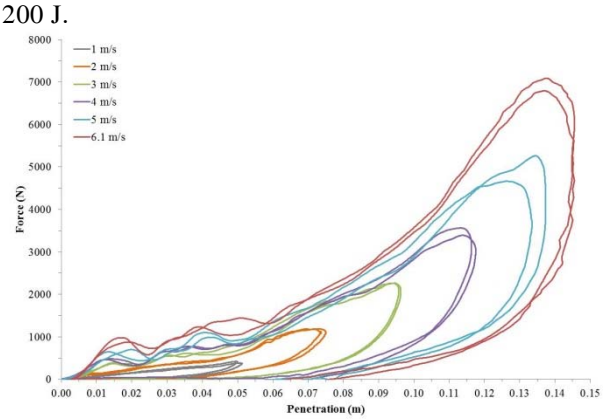

Figure 18. Prototype abdomen force-penetration responses under 32 kg rigid-bar impacts for impact speed ranging from 1 to 6.1 m/s.

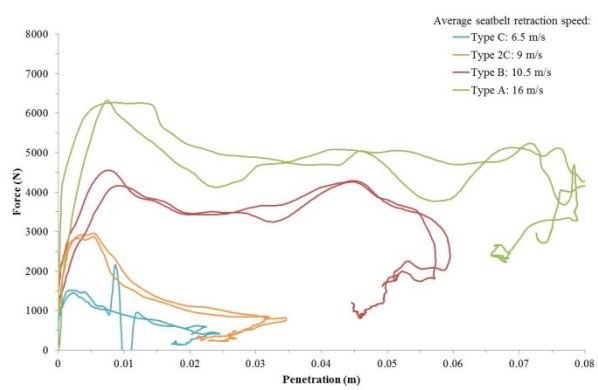

Figure 19. Prototype abdomen force-penetration responses under pretensioners Type C, 2C, B and A.

APTS measurements

Figure 20 to Figure 23 show APTS pressure versus abdomen penetration for rigid bar impacts and seatbelt loading. Under seatbelt loading, the pressure peaks are observed at the beginning of the penetration. The APTS pressure peaks occur between 10 mm (pretensioner Type C) and 35 mm (pretensioner Type A) penetration. Figure 24 and Figure 25 reveal that pressure peaks are synchronized with force peaks in the case of the prototype without the small masses and delayed by around 4 ms in the case of the prototype. Indeed, with the little masses, the first force peak is linked to the masses inertia whereas there is little abdomen penetration.

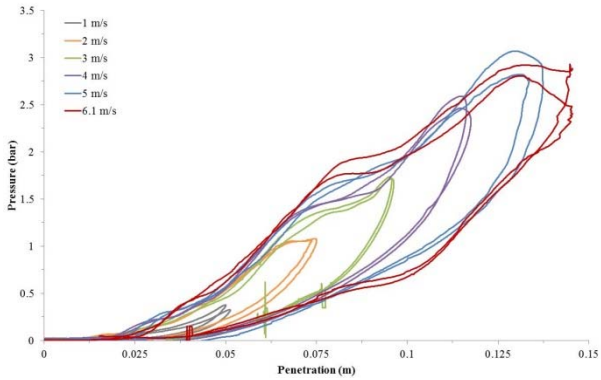

Figure 20. Left APTS pressure versus abdomen penetration for rigid-bar impacts from 1 to 6.1 m/s.

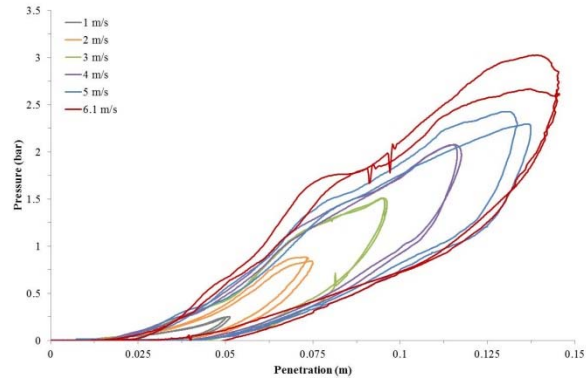

Figure 21. Right APTS pressure versus abdomen penetration for rigid-bar impacts from 1 to 6.1 m/s.

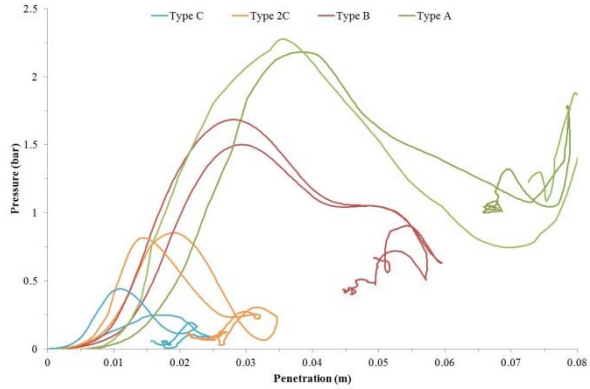

Figure 22. Left APTS pressure versus abdomen penetration for seatbelt loading using pretensioner Type C, 2C, B and A.

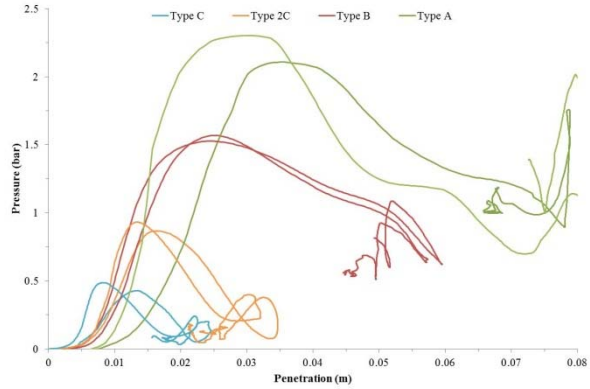

Figure 23. Right APTS pressure versus abdomen penetration for seatbelt loading using pretensioner Type C, 2C, B and A.

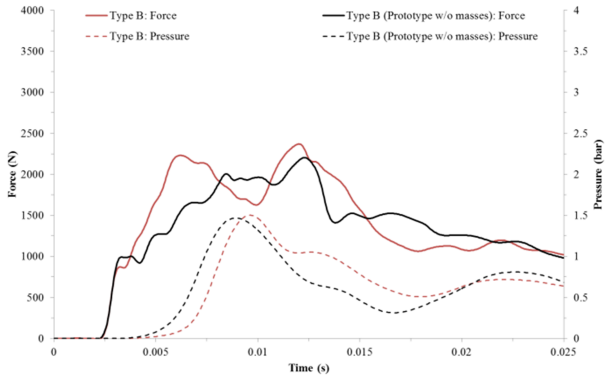

Figure 24. Left seat belt force (y-axis1) and left APTS pressure (y-axis2) versus abdomen penetration for pretensioner Type B.

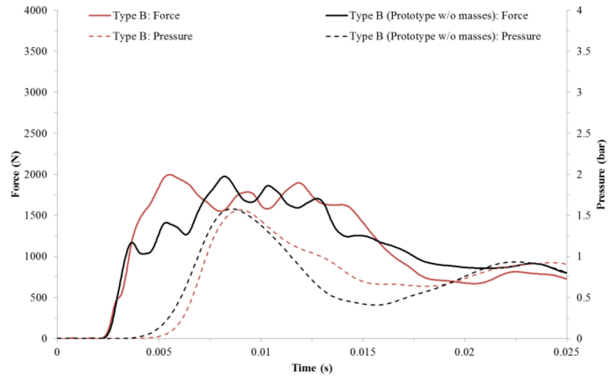

Figure 25. Right seat belt force (y-axis1) and right APTS pressure (y-axis2) versus abdomen penetration for pretensioner Type B.

Rigid-bar impacts performed with the dummy rotated by 20° to its left side, exposing more the right APTS, showed the ability of the APTS to discriminate the loading direction. Almost twice higher pressure peaks were recorded by the right APTS (Figure 26).

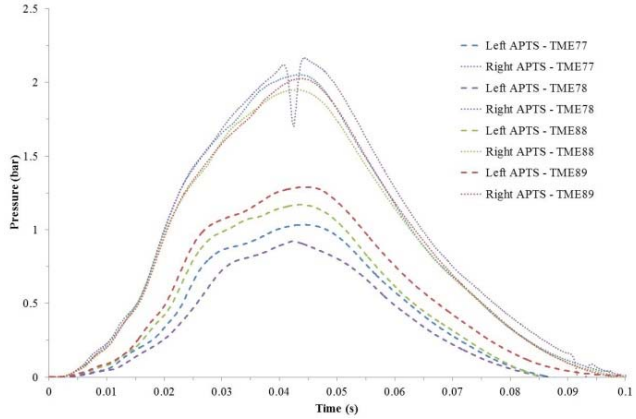

Figure 26. Left and right APTS pressure for 20° rigid-bar impacts at 3 m/s (4 tests).

DISCUSSION

Biofidelity The prototype biofidelity was improved under rigid-bar impacts thanks to the addition of the small masses and the higher stiffness of the APTS compared to the front foam. The increased abdominal depth in the prototype made the contact between the rigid-bar and the pelvis flesh occurring later than with the THOR-NT abdomen. In the THOR-Mod Kit and THOR-Metric (most recent version of THOR released by NHTSA), the pelvis flesh at the antero-superior iliac spine (ASIS) are shortened by 20 mm. It is therefore expected that such contact with the rigid-bar impact will not occur anymore. It will remain that the stiffness observed between 90 and 120 mm penetration is still higher than PMHS corridors. This might be solved by changing the abdominal rear foam block properties.

The human response under the seatbelt/pretensioner loading is much more challenging to mimic. The force can be increased, but not to a sufficient level compared to PMHS. The penetration remains lower than that of the PMHSs. A comparison between the prototype and the average scaled PMHS response under pretensioner Type B gives further insight into these differences compared to the corridor (Figure 27-Left). A similar curve shape is in fact observed but it appears that the force plateau after the initial force peak is longer for the prototype (around during 15 mm penetration compared to 5 mm for the PMHSs). A second higher force plateau exists for the PMHS response whereas the penetration of the prototype is stopped. It is therefore necessary to reduce the first plateau in the prototype and increase the force between 20 and 50 mm penetration. This might be done by changing the front foam characteristics to a stiffer material.

Finally, the first force peak should be at the really beginning of the impact (Figure 27). This should be achieved by placing the small masses inside the dummy suit instead of the surface of the abdomen Cordura bag.

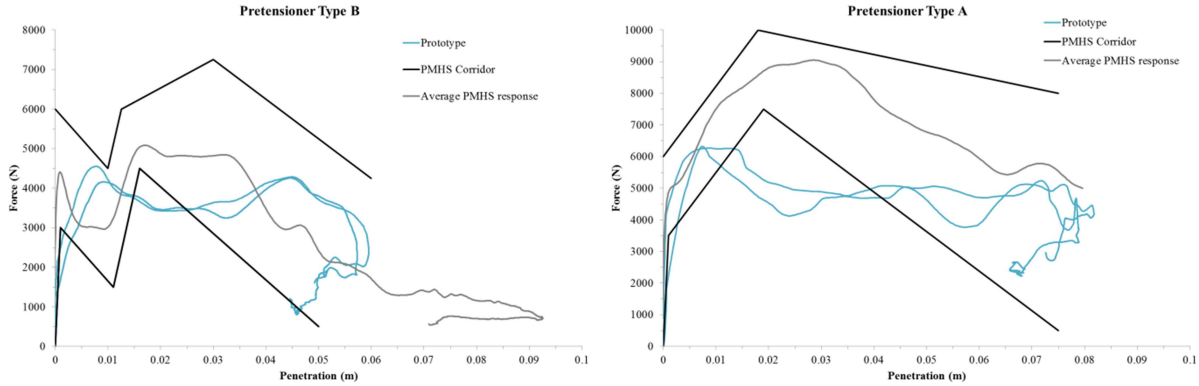

Figure 27. Force-penetration response of the prototype compared to Foster et al. (2006) PMHS corridors and average PMHS response scaled with Eppinger technique (Lebarbé, 2011)(Left: Type B, Right: Type C).

Instrumentation The abdomen prototype is equipped with two APTSs. In THOR-Mod Kit and THOR-Metric, the pelvis ASISs are equipped with load cells (Ridella et al., 2011). This will provide information on the lap belt and the pelvis interaction in addition to the lap belt and abdomen interaction given by the APTS. The pressure peaks measured by the APTSs corresponded to the force and the penetration peaks measured under the rigid-bar impacts (Table A 1). Under the seatbelt loading, the pressure peak corresponded to the force peak in the prototype without the small masses (Figure 24 and Figure 25). In the prototype (including the small masses), this is not the case as explained earlier. Regarding the penetration peak, there is always a significant time delay (around 10 ms) between the pressure and the penetration peaks as between the force and the penetration peaks (Table A 2). The pressure curves follow force history curve shapes.

Injury prediction Cavanaugh et al. (1986) PMHS tests led to abdominal AIS4 injuries for speeds higher than 6 m/s. In Foster et al (2006) study, only tests with pretensioner Type A created AIS2 to AIS3 abdominal injuries. In these two test configurations, the APTS pressure peaks were above 2.7 bars and 2 bars respectively. Beillas et al. (2012) estimated a threshold of 1 bar for the child Q-dummies. This is of course not possible to compare since the tolerance of adult and child is certainly different and since the dummy abdomen designs are also different.

CONCLUSIONS

The APTSs already used in 3 and 6 years old Q-dummies were introduced into THOR lower abdomen front foam block. Small masses were added on the abdomen Cordura bag and the assembly was mounted on THOR-NT dummy. The response of the abdomen prototype was then compared to the THOR-NT abdomen and to PMHS corridors under 6.1 m/s rigid-bar impact and Foster's seatbelt/pretensioner loadings. Generally, the force-penetration response of the prototype was closer to PMHS response and the APTS pressures accounted well for the impact severity as measured by external force measurements or dummy abdominal penetration. Along the analysis, below proposals were made to further improve the abdomen response:

1. Moving the small masses inside the dummy suit to create earlier the initial peak force seen on PMHS responses,
2. Changing rear foam block properties to a softer material to allow a larger penetration and a lower force after 90 mm penetration,
3. Increasing front foam stiffness to raise further force up to 50 mm penetration,
4. Proceeding with 2/ and 3/ above might lead to using a single lower abdominal foam block since the front foam is too soft and the rear foam is too stiff.

In the component tests performed in this study, the interaction between the pelvis flesh and the rigid-bar or the seatbelt webbing influenced largely the results. This could be easily identified in the rigid-bar tests but less easily in the seatbelt tests. The THOR-Metric is equipped with ASIS load cell and its pelvis flesh has been shortened by around 20 mm. Together with the prototype abdomen, THOR-Metric will allow measurement of the load applied to the pelvis and to the abdomen, discretely.

Interaction between the lower abdomen and the upper torso will need to be considered. Evaluation in sled tests highlighted that further work is also needed to understand the influence of the dummy kinematics on the pressure measurements.

REFERENCES

Beillas P., Alonzo F., Chevalier M-C., Lesire P., Leopold F., Trosseille X., Johannsen H. (2012) Abdominal twin pressure sensors for the assessment of abdominal injuries in Q dummies : In-dummy evaluation and performance in accident reconstruction. Stapp Car Crash Journal 56: 387-410.

Cavanaugh J. M., Nyquist G. W., Goldberg S. J., King A. I. (1986) Lower abdominal tolerance and response. Proceedings of 30th Stapp Car Crash Conference, pp. 41-63, SAE technical paper No 861878. Society of Automotive Engineers, Warrendale, PA.

Eppinger R. H. (1976) Prediction of thoracic injury using measurable experimental parameters. Proceedings of 6th international ESV Conference, p. 770. Washington, DC, USA. 1976.

Foster C. D., Hardy W. N., Yang K. H., King A. I. (2006) High-speed seatbelt pretensioner loading of the abdomen. Stapp Car Crash Journal 50: 27-51.

Frampton R., Lenard J., Compigne S. (2012) An in-depth study of abdominal injuries sustained by car occupants in frontal crashes. Proceedings of 56th Association for the Advancement of Automotive Medicine, Chicago, Illinois. October, 2012.

Hanen G., Bermond F., Compigne S., Masuda M. (2011) Contribution to the improvement of crash test dummies in order to decrease abdominal injuries in road accidents. Proceedings of 22nd international ESV Conference, Paper No 11-0218. Washington, DC, USA. June 13-16, 2011.

Hanen G, Vezin P., Bermond F., Masuda M., Compigne S. (2012) A pressure-based abdominal insert for THOR-NT. JSAE Annual Congress, Pacifico Yokohama, Japan. May 2012.

Hardy W. N., Schneider L. W., Rouhana S. W. (2001) Abdominal impact response to rigid-bar, seatbelt, and airbag loading. Stapp Car Crash Journal 45: 1-31.

Huelke D. F., Mackay G. M., Morris A. (1993) Intraabdominal injuries associated with lap-shoulder belt usage. SAE paper n°930639.

Kent R., Stacey S., Kindig M., Woods W., Evans J., Rouhana S. W., et al. (2008) Biomechanical response of the pediatric abdomen, Part 2: Injuries and their correlation with engineering parameters, Stapp Car Carsh Journal 52: 135-166.

Klinich K. D., Flannagan C. A., Nicholson K. et al. (2008) Abdominal injury in motor vehicle crashes. UMTRI technical report UMTRI-2008-40.

Kremer M. A., Gustafson HM, Bolte J. H., Stammen J., Donnelly B. (2011) Pressure-based abdominal injury criteria using isolated liver and full-body post-mortem human subject impact test. Stapp Car Crash Journal 55: 317-350.

Lamielle S., Cuny S., Foret-Bruno JL., Petit P., Vezin P., Verriest JP., Guillemot H. (2006) Abdominal injury patterns in real frontal crashes: Influence of crash conditions, occupants seat and restraint systems. Association for the Advancement of Automotive Medicine, Chicago, Illinois. October 16-18, 2006.

Lamielle S., Vezin P., Verriest JP., Petit P., Trosseille X., Vallancien G. (2008) 3D deformation and dynamics of the human cadaver abdomen under seatbelt loading. Stapp Car Crash Journal 52: 267-294.

Lebarbé M. (2011) Contribution to the definition of biofidelity corridors in frontal impact for an adult male 50th percentile – Abdomen. ACEA report Revision 9. September 2011.

Martin JL., Lardy A., Compigne S. (2010) Specificities of rear occupant protection: Analysis of French accident data. Proceedings of IRCOBI Conference, Hanover. September 2010.

Masuda M., Compigne S. (2012) Dynamic response of the THOR-NT: Thorax and Abdomen. SAE 2012. Government/industry meeting. Washington, DC, USA. January 25-27, 2012.

Miller M.A. (1989) The biomechanical response of the lower abdomen to belt restraint loading. Journal of trauma 29 (11): 1571-1584.

National Highway Traffic Safety Administration, THOR-NT user manual 50% male frontal dummy, Revision 2005.1, Report No: GESAC-05-02, U.S. Department of Transportation, Washington, DC, March 2005.

Parent D. P. (2014) Applications of the THOR ATD in NHTSA research. . SAE 2014. Government/industry meeting. Washington, DC, USA. January 22-24, 2014.

Ridella S. A., Parent D. P. (2011) Modifications to improve the durability, usability and biofidelity of the THOR-NT dummy. Proceedings of 22nd international ESV Conference, Paper No 11-0312. Washington, DC, USA. June 13-16, 2011.

Ruan J. S., El-Jawahri R., Barbat S., Prasad P. (2005) Biomechanical analysis of human abdominal impact responses and injuries through finite element simulations of a full human body model. Stapp Car Crash Journal 49: 343-366.

Trosseille X., Le-Coz JY., Potier P., Lassau JP. (2002) Abdominal response to high-speed seatbelt loading. Stapp Car Crash Journal 46: 71-79.

APPENDIX I

Table A 1. Peak values and timing in rigid-bar impacts.

		Rigid-bar impact			
Impact speed (m/ss)	**Test Id**	**Force (N) @ Time (ms)**	**Penetration (mm) @ Time (ms)**	**Left Pressure (bar) @ Time (ms)**	**Right Pressure (bar) @ Time (ms)**
1	TME82	384@75	51@84	0.33@79.2	0.25@76.9
	TME83	419@73.3	50@79.5	0.38@75.2	0.25@75.2
2	TME84	1183@44.2	74@55	1.1@51.3	0.9@50.4
	TME85	1185@47.1	75@56.5	1.1@51.8	0.8@51.1
3	TME79	2263@41.8	96@47	1.7@43.6	1.5@43
	TME80	2265@41.8	96@47	1.7@44	1.5@42.4
4	TME90	3563@35.3	116@40.5	2.6@36.9	2.1@37.3
	TME91	3389@36	118@42.5	2.5@36.7	2.1@37.4
5	TME92	4661@30.9	134 @38	2.8@34.5	2.4@33.3
	TME93	5261@33.7	137@39	3.1@30.8	2.3@35.4
6.1	TME94	6791@27	146@35	2.8@25	3.0@28
	TME95	7088@26.6	146@32	2.9@33.7	2.7@26.3

Table A 2. Peak values and timing in seatbelt loading.

		Seatbelt loading				
PT	**Test Id**	**Left Force (N) @ Time (ms)**	**Left Pressure (bar) @ Time (ms)**	**Right Force (N) @ Time (ms)**	**Right Pressure (bar) @ Time (ms)**	**Penetration (mm) @ Time (ms)**
Type C	TAP39	563@4.6	0.25@11.6	888@4.5	0.43@9.9	17@20.5
	TAP40	730@6.1	0.44@10.6	917@4.6	0.49@9.3	23@19
Type B	TAP41	2370@12 (*)	1.5@9.6	1996@5.5	1.6@9	57@16.5
	TAP42	2479@12.2 (*)	1.7@9.7	2278@5.7	1.5@9.3	60@17
Type 2C	TAP43	1616@5.1	0.85@8.6	1346@5.2	0.87@8.2	35@17
	TAP44	1592@4.5	0.82@9.2	1315@5.3	0.9@8.8	32@16.5
Type A	TAP45	3492@3.8	2.2@7.9	2832@3.7	2.1@7.6	79@23
	TAP46	3480@3.8	2.3@7.4	3166@4.8	2.3@6.8	82@16.5

(*) This time corresponds to the second peak force. The first one is slightly lower but occurs at 6 ms.